



Journal of Mining and Environment (JME)

journal homepage: [www.jme.shahroodut.ac.ir](http://www.jme.shahroodut.ac.ir)



## Adsorptive Study of Cadmium Removal from Aqueous Solution Using a Coal Waste Loaded with Fe<sub>3</sub>O<sub>4</sub> Nanoparticles

Sasan Mirshrkari, Vahideh Shojaei\*, and Hamid Khoshdast

Department of Mining Engineering, Higher Education Complex of Zarand, Zarand, Iran

### Article Info

Received 19 April 2022

Received in Revised form 20 May 2022

Accepted 8 June 2022

Published online 8 June 2022

[DOI:10.22044/jme.2022.11796.2174](https://doi.org/10.22044/jme.2022.11796.2174)

### Keywords

Coal waste

Fe<sub>3</sub>O<sub>4</sub> nanoparticles

Nanocomposite

Cadmium

Kinetics

### Abstract

A coal waste sample loaded with Fe<sub>3</sub>O<sub>4</sub> nanoparticles is employed as an efficient adsorbent to remove Cd from synthetic wastewater. The synthesized nanocomposite is characterized using the Fourier transform-infrared (FT-IR), X-ray diffraction (XRD), and transmission electron microscopy (TEM) techniques. The visual analysis of the microscopic image shows that the mean size of the magnetite nanoparticles is about 10 nm. The effects of the operating variables of the initial solution pH (3-11) and nanocomposite to pollutant ratio (7-233) are evaluated using the response surface methodology on cadmium adsorption. The process is also optimized using the quadratic prediction model based on the central composite design. The statistical analysis reveals that both factors play a significant role in Cd adsorption. The maximum Cd removal of 99.24% is obtained under optimal operating conditions at pH 11 and nanocomposite/cadmium ratio of 90 after 2 h of equilibrium contact time. A study of the adsorption kinetics indicates that the maximum removal could be attained in a short time of about 2 min following a first-order model. The isotherm investigations present that the Cd adsorption on the Fe<sub>3</sub>O<sub>4</sub>/coal waste nanocomposite has a linearly descending heat mechanism based on the Temkin isotherm model with the minor applicability parameters than the other isotherm models. The overall removal behaviour is attributed to a two-step mechanism including a rapid adsorption of cadmium ion onto the active sites at the surface of nanocomposite followed by a slow cadmium hydroxide precipitation within the pores over the nanocomposite surface.

### 1. Introduction

In the current industrial world, pollution of water resources and habitats by industrial pollutants is one of the major concerns of the environmental activists. Among the types of pollutants, heavy metals are more critical due to their high reactivity and stability, as well as significant health hazards [1]. In this regard, several methods such as filtration, reverse osmosis, adsorption, and membrane removal have been developed to treat water contaminated with these heavy pollutants [2]. Among the various treatment methods, the adsorption processes have found broader applications in polluted water treatment industries due to their ease of operation and more mature knowledge. However, the

efficiency of this method depends significantly on the quality and efficiency of the adsorbent. Therefore, considerable efforts have been made to produce or improve the adsorption properties of natural to synthetic adsorbents [3].

In the recent years, the quality improvement of conventional adsorbents used in the water treatment industry has received much attention from the researchers in the light of significant advances in nanotechnology. Regardless of the type of nanoscale adsorbents, the modification of microscale adsorbents with nanomaterials is significant for producing composite adsorbents called nanocomposites. Many studies have been conducted to synthesize and characterize such

✉ Corresponding author: [v.shojaei@uk.ac.ir](mailto:v.shojaei@uk.ac.ir) (V. Shojaei).

nanocomposites during the last decade. For example, Wei *et al.* [4] have studied the adsorptive properties of montmorillonite coated by carbon to remove Cr (VI) from aqueous solutions. The results obtained demonstrated that their nanocomposite might show different removal efficiency by varying pH values. They performed an extensive instrumental analysis to explore the adsorption mechanisms, and showed that a multiplicity of phenomena including electrostatic attraction, precipitation, ion reduction, and complexation are involved in removing chromium ions by the developed nanocomposite. Singh and Rachna [5] have reported the efficient removal of Cr(VI) from wastewater using nanocomposites, indicating that copper ferrite/polyaniline nanocomposites could be considered a promising adsorbent for the environmental remediation purposes. Dinh *et al.* [6] have demonstrated that the chitosan/MnO<sub>2</sub> nanocomposites can efficiently treat chromium-contaminated water under highly acidic conditions, and provide an appropriate adsorption time (120 min). Zhang *et al.* [7] have evaluated the adsorption properties of a nanocomposite based on graphene oxide and montmorillonite for the simultaneous treatment of Pb<sup>2+</sup>/p-nitrophenol-polluted wastewaters, showing over 98% of lead ions removal in a competitive environment. The treatment of lead-polluted waters has also been evaluated with nanofibrous polycaprolactone nanocomposite enhanced by clay and zeolite nanoparticles [8]. Regardless of the removal efficiency, adding such nanoparticles to nanofibrous polycaprolactone has resulted in some synergistic interactions with the adsorption capacity of the nanocomposite. Akbarzadeh *et al.* [9] have indicated that nanocomposites produced using zeolitic imidazolate frameworks and nickel titanate could be an efficient adsorbent for removing lead ions from wastewater with the maximum adsorption capacity of 155 mg.g<sup>-1</sup>. The same results have been observed elsewhere by Wu *et al.* [10], who have used Fe<sub>3</sub>O<sub>4</sub> instead of nickel titanate for synthesizing their nanocomposite to treat water contaminated with copper and arsenic ions. Jung *et al.* [11] have examined the application of hydroxyapatite/biochar nanocomposites to remove cupric ions from wastewater, and have shown its promising capability as a low-cost and eco-friendly adsorbent for treating contaminated aqueous media. Other researchers have also studied the use of carbon-based nanocomposites. For example, Alhan *et al.* [12] have used nanocomposites of

ZnO/activated carbon to treat wastewater from cadmium ions. They showed that numerous factors might affect the removal efficiency such as the solution pH, adsorbent/adsorbate ratio, and contact time. It was experimentally demonstrated that ZnO/activated carbon nanocomposites could be served as an efficient adsorbent in the actual industrial scales. Similar results have been observed by Chen *et al.* [13], who have used MoS<sub>2</sub>/lignin-derived carbon nanocomposites to efficiently eliminate Cr (VI) from wastewaters. They showed that the adsorption mechanism was controlled by both adsorption and reduction.

Iron oxide nanoparticles are productive enhancers for synthesizing different types of nanocomposites. Gupta and Nayak [14], for example, have modified an agricultural waste-orange peel powder into a novel magnetic nano-adsorbent by co-precipitating it with Fe<sub>3</sub>O<sub>4</sub> nanoparticles (MNP) for cadmium ion removal from aqueous solutions. They showed that cadmium removal was achieved at 82% from a simulated electroplating industry wastewater. In another research work, Gong *et al.* [15] have used magnetic nanoparticles as the bed for producing a nanocomposite for the removal of cadmium from wastewaters. The nanocomposite synthesis was performed by coating a shellac layer, a natural biodegradable and renewable resin with abundant hydroxyl and carboxylic groups, on the surface of iron oxide magnetic nanoparticles. However, they reported that a low adsorption capacity of 18.80 mg/g was obtained for the treatment experiments. Cadmium ion removal from aqueous solutions using alumina/iron oxide nanocomposite has also been examined by Abd El-Latif and co-workers [16]. They showed that their nanocomposite could effectively treat Cd (II)-contaminated wastewater through an endothermic process. Recently, advanced nanocomposites have been produced by coupling magnetic nanoparticles and other metal, either individually or as oxide. Banerjee *et al.* [17], for example, have synthesized a core-shell Fe<sub>3</sub>O<sub>4</sub>/Au nanocomposite to remove arsenic (III) from wastewater. They illustrated that their nanocomposite adsorbent could yield about 70% of As (III) removal under optimal conditions. In another study, Eslami *et al.* [18] have used a Fe<sub>2</sub>O<sub>3</sub>/Mn<sub>2</sub>O<sub>3</sub> nanocomposite with polytitanium chloride being present to efficiently treat an As (III)-contaminated wastewater under optimal conditions. There are many other double-phase nanocomposites that have been successfully applied to the remediation of aqueous environments contaminated by heavy metals such

as  $\text{Ti}_3\text{C}_2\text{T}_x$ /polyethyleneimine nanocomposites [19], activated carbon of lemon/ $\text{Fe}_3\text{O}_4$  magnetic nanocomposite [20],  $\text{Fe}_3\text{O}_4$ /CAC nanocomposite [21], nano-zero-valent iron nanoparticles/clinoptilolite natural zeolite nanocomposite [22], cellulose acetate/Sn(IV) iodophosphate nanocomposite [23],  $\beta$ -Cyclodextrin/ $\text{ZrO}_2$  nanocomposite [24], and graphene oxide/nickel ferrite nanocomposite [25].

Nanocomposite can also be prepared from even more than two phases, i.e. bed material and only a single nano-enhancer. For example, Ghaeni *et al.* [26] have investigated the adsorptive performance of a  $\text{Fe}_3\text{O}_4/\text{MnO}_2$ /fulvic acid nanocomposite to treat seawater from strontium ions, which serves as an excellent adsorption with a significant capacity of  $227.3 \text{ mg.g}^{-1}$ . Li *et al.* [27] have studied the effects of numerous operating conditions including solution pH, temperature, initial concentration of adsorbate, and adsorption time on chromium removal from wastewater using magnetic illite/smectite nanocomposite enhanced with ternary polyethyleneimine. In addition to the acceptable adsorption efficiency, the nanocomposite can still preserve over 71% of its initial activity for further adsorption purposes even after six cycles. Some other researchers have recently demonstrated the high adsorption performance of multi-component nanocomposite. For example, Reis *et al.* [28] have shown that Cr (VI)-contaminated wastewater can be treated using maghemite/chitosan/polypyrrole nanocomposite under optimal conditions in at least five cycles without any substantial loss in its initial adsorption capacity. As Sarojini and co-workers have reported, lead cations are also highly removed from heavy metal-bearing water using polypyrrole/ $\text{Fe}_2\text{O}_3$ /seaweed nanocomposite [29]. EDTA/functionalized graphene oxide/chitosan nanocomposite [30], polyphenols/functionalized graphite/hematite nanocomposite [31], and hybrid silica aerogel (HSA)/ $\text{Fe}_3\text{O}_4$ /chitosan nanocomposite [32] may also be mentioned, among other nanocomposites consisting of more than two phases for the efficient treatment of heavy metal contaminated wastewaters.

The  $\text{Fe}_3\text{O}_4$  modified nanocomposites based on carbon materials have also shown a promising applicability in decontamination of heavy metal pollutants from aqueous solutions. For instance, Xu and co-workers [33] have shown that nanocomposites produced from chitosan encapsulated magnetic  $\text{Fe}_3\text{O}_4$  nanoparticles can effectively remove cadmium ion from wastewater

with a significant adsorption capacity of 200 mg/g. Successful results have also been reported by Kang *et al.* [34] who used a magnetic acid-treated activated carbon nanocomposite to remove some heavy metals from aqueous solutions. They showed that maximum adsorption capacities of 49.8 and 86.2 mg/g for cadmium and lead could be achieved under optimal conditions. In another work, the adsorption capacity of a magnetic biochar composite for the removal of cadmium from wastewater has been assessed [35]. The results revealed that the produced magnetic biochar was viable for adsorption of both heavy metal ions and organic pollutant at optimised condition. Recently, Zubrik and co-workers have examined the mechanochemically-synthesised coal-based magnetic carbon composites for removing Cd (II) from aqueous solutions [36]. They showed that adsorption capacity of the nanocomposite could vary based on the type of the clean coal used as the base material, e.g. 70.4 mg/g and 58.8 mg/g for lignite- and char-based nanocomposites, respectively.

The above studies have been published on developing and applying nanocomposites for wastewater treatment. Regardless of the variety of synthesized composites, their adsorption properties and effectiveness were improved compared to the individual adsorbents. There are hundreds of coal washing plants around the world that produce and dispose millions of tons of coal tailings in tailing dams and dumping sites. These rejected coal products face the environment with various health hazards due to their contained heavy metal, sulfur and fines and possibly, nano-minerals. However, coal tailings are abundant mining waste that can be employed as a low-cost and available absorber to remove environmental pollutants [3]. With respect to this potential applicability, the current study aims to use a coal waste sample as bedrock for producing a  $\text{Fe}_3\text{O}_4$ -based nanocomposite to improve the treatment efficiency of cadmium-polluted aquatic environments. Different instrumental analysis techniques were utilized to characterize the synthesized nanocomposite. The main effects and interactions among the selected operating factors influencing the efficiency of cadmium removal including the initial pH of the solution and nanocomposite to ion ratio were assessed using systematically designed experiments. The kinetics and adsorption models of Cd(II) ion adsorption were also investigated. To the authors' best knowledge, this is the first report on the synthesis

and application of nanocomposites based on coal wastes.

## 2. Materials and Methods

### 2.1. Sampling and characterization of coal waste

The coal waste sample used in this research work was carefully sampled from the fine tailings pool of a coal beneficiation plant in Zarand, Iran. A representative sample of 200 g was first prepared using standard sample preparation techniques for the coal waste chemical and physical characterization. The particle size distribution of the waste sample was indicated using the wet sieve analysis method by the screen set from 500  $\mu\text{m}$  to 50  $\mu\text{m}$ . The content of noncombustible materials of waste was measured according to the ASTM D 3174-73 standard. The chemical composition and surface morphology of the sample were also studied using X-ray diffraction (XRD, Philips, X'pert-MPD system) and scanning electron microscopy (SEM, Tescan, Vega-II microscope), respectively.

### 2.2. Magnetite-coal waste nanocomposite production

Approximately 12 mL of 2 M  $\text{FeCl}_2 \cdot 4\text{H}_2\text{O}$  solution and 48 mL of 1 M  $\text{FeCl}_3 \cdot 6\text{H}_2\text{O}$  solution were first added to a 1 L beaker filled with 180 mL of deionized water to synthesize the  $\text{Fe}_3\text{O}_4$  nanoparticles, and then 350 mL of 1 M  $\text{NH}_3$  solution was added to the solution by titration for 5 min [37]. Then 18 g of coal waste was added to the mixture and stirred for 3 h at 60 °C on a magnetic stirrer at 200 rpm to produce the two-phased nanocomposite. The synthesized product was then filtered and dried at the ambient temperature for further use.

### 2.3. Characterization of nanocomposite

Some instrumental experiments were employed to identify the morphological and physical characteristics of the synthesized nanocomposite. The Fourier transform-infrared (FT-IR) spectrum of the nanocomposite was measured over the region of 400–4000  $\text{cm}^{-1}$  via TENSOR 27 (Brucker) using KBr pellets. Transmission electron microscopy (TEM, LEO 912AB, LEO) and X-ray diffraction (XRD, Philips, X'pert-MPD system) were used to study the quality and quantity of the synthesized nanocomposite.

### 2.4. Adsorption experiments

A multiplicity of statistical designs was developed to construct an experimental program to assess the behaviour of any particular process when the operational conditions were required to be varied within a predefined range. Among the available experimental designs, the response surface methodology (RSM) is well-known as powerful DOEs providing a reasonable amount of information by which the engineer can evaluate the way, either linear or non-linear. The selected operating variables may affect the process response(s), as well as the potential interaction among them [38]. Generally, two types of RSMs can assess the experimental space, central composite (CCD), and Box-Behnken (BBD) designs. CCD uses a limited number of extrapolated levels for operating variables to predict the response space of the process, while BBD employs interpolated levels for the same target. Therefore, CCDs are functional designs for developing the prediction models, whereas BBDs help monitor small variations in process response(s), and the operating variables are changed within their levels [39]. There are numerous parameters that may influence the performance of the adsorption process, among which solution pH, concentration of pollutant in aqueous solution, adsorbent dose, and contact time are of key importance. Therefore, in this work, the DOE approach was considered first to assess the effects of the selected operating variables, namely initial solution pH and nanocomposite/ion ratio (F/M), on cadmium removal as the process response and optimize the operational conditions to reach the maximum adsorption.

Given that the analysis of experimental designs is based on modelling the behaviour of the process response(s) to the operational parameters, so selecting the optimal number of model variables is very important. Generally, using a large number of variables complicates the relationship between the response and the variables and reduces the accuracy of the model. For this reason, in this work, the two variables of pollutant concentration and adsorbent dose were combined with each other and examined as a dimensionless ratio of nanocomposite to ion. Using dimensionless ratios instead of dimensional parameters has two key advantages: first, it simplifies modelling and understanding effects, and next, it allows the optimal value of a parameter to be easily determined by changing another individual parameter involved in the ratio i.e. ion

concentration or adsorbent dose in this work [40]. Therefore, the experimental investigation was planned based on the central composite design and structure levels (Tables 1 and 2). In addition, since no similar research work has been reported so far, the range of variable levels has been considered wide enough to monitor the adsorption performance behaviour more accurately under the influence of the operational parameters. The extrapolation values in Table 1 were determined by the Design-Expert software based on the relevant statistical calculations. The high levels of ion-to-adsorbent levels are due to the arithmetic fractionation of the adsorbent dose to the initial cadmium concentration, which has been reported in other studies (e.g. [3, 41]).

For each experimental run, requisite amounts of the nanocomposite were added to a beaker containing 200 mL of aqueous solution polluted with cadmium with a concentration of 100 ppm. Then the solution pH was adjusted based on the experimental design by adding 0.1 M solution of HCl and NaOH. Afterward, the mixture was agitated at 180 rpm and left for 2 h to ensure a perfect adsorption process [3]. Based on the results presented in the literature, some of which

were reviewed in the introduction, the absorption processes usually occur in less than an hour. For this reason, in this work, time was not considered as a primary variable in the experimental design. Rather, its effect was studied in detail in process kinetics studies, and the optimal process time to achieve maximum removal efficiency was determined. Finally, the mixture was filtered, and the residual liquid phase was analysed for cadmium concentration. All tests were performed at the ambient temperature. The equilibrium and kinetic studies were further performed during the optimum test after process optimization. The cadmium concentration in each incremental sample taken during adsorption experiments was measured using atomic absorption analysis (Varian model SpectAA 220, Mulgrave, Victoria). Then the efficiency of the treatment process,  $R_{Cd}$ , was calculated using the following equation [41]:

$$R_{Cd} = \frac{(C_0 - C_t)}{C_0} \times 100 \quad (1)$$

where  $C_0$  and  $C_t$  are the initial and final concentrations of ion in the solution, respectively.

**Table 1. Operating variables and their levels selected for construction of adsorption experimental design.**

Adsorption variables	Lower Ex. Level	Low level	Middle level	High level	Higher Ex. Level
A: pH	2.75	4	7	10	11.24
B: F/M ratio	6.86	40	120	200	233.14

**Table 2. CCD developed for adsorption studies and their corresponding experimental results.**

Run	A:pH	B:F/M ratio	Cd Removal (%)
1	10	200	96.85
2	4	40	33.17
3	7	120	55.89
4	4	40	30.67
5	7	233.14	75.35
6	11.24	120	99.27
7	2.75	120	30.82
8	4	200	52.42
9	7	120	55.71
10	7	6.86	24.82
11	7	233.14	76.42
12	10	200	96.90
13	7	120	51.96
14	2.75	120	28.48
15	10	40	91.16
16	7	6.86	28.26
17	11.24	120	99.33
18	7	120	59.10
19	7	120	57.67
20	10	40	91.35
21	4	200	49.92
22	7	120	57.67

### 3. Results and Discussion

#### 3.1. Results of characterization studies

Sieve analysis indicated that the coal waste sample had a characteristic top size ( $d_{95}$ ) finer than 100  $\mu\text{m}$ . The ash analysis showed that the noncombustible material constitutes 65.14% of the waste sample. The SEM image of the coal waste sample is presented in Figure 1, indicating that the waste sample includes angular particles having no unusual surface patterns and excess void spaces. The XRD pattern of the waste sample (Figure 2) reveals that the noncombustible materials mainly consist of biotite and quartz as major phases and calcite as a minor phase. The quantitative analysis of the XRD result is presented in Table 3.

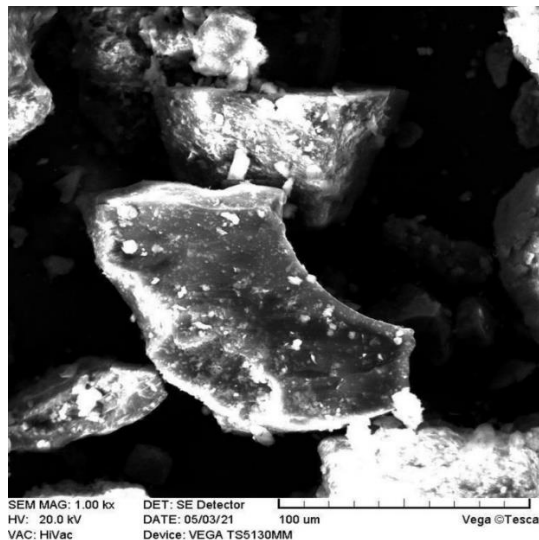


Figure 1. Morphology of coal waste particles identified by SEM method.

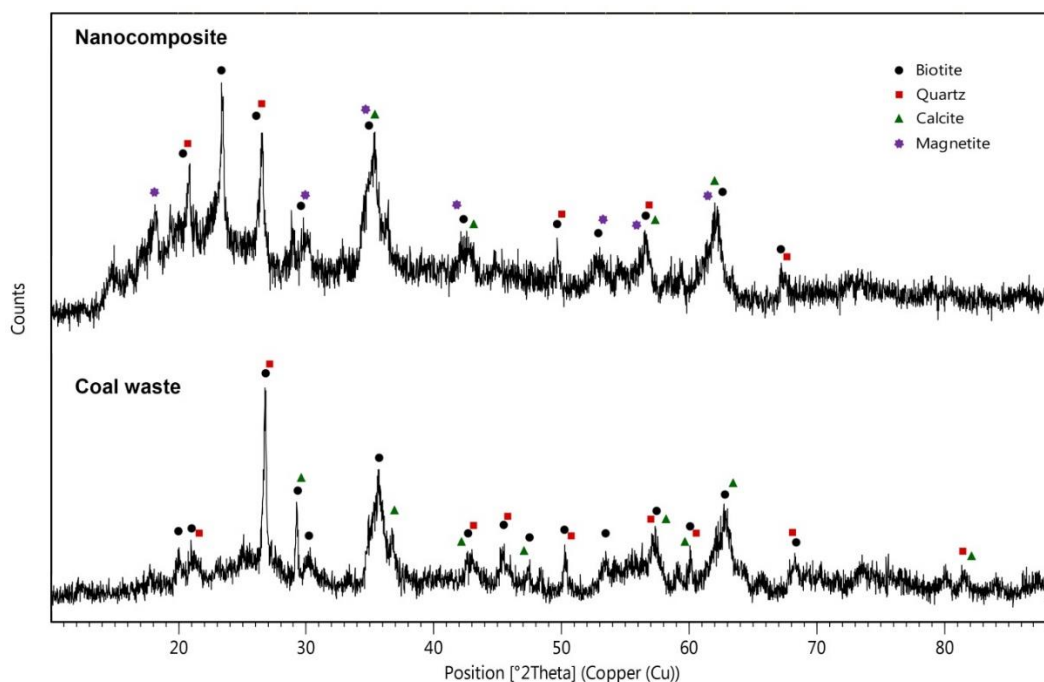


Figure 2. XRD patterns of coal waste sample and synthesized nanocomposite.

Table 3. Percentage of mineralogical phases in coal waste and synthesized nanocomposite.

	Biotite	Quartz	Calcite	Magnetite
Coal waste	36	58	6	ND*
Nanocomposite	50.4	33.7	3	12.9

\* Not detected

The FT-IR spectrum of the synthesized nanocomposite, shown in Figure 3, presents a wideband located at around 3400  $\text{cm}^{-1}$  that corresponds to O–H stretching [42]. A very low-intensity band corresponds C–H stretching vibration at 2920  $\text{cm}^{-1}$ . Another characteristic band is indicated around 1400  $\text{cm}^{-1}$  due to the –C–H bending vibration. Around 1615  $\text{cm}^{-1}$ , a band

corresponds to C=O stretching vibration, and around 1030  $\text{cm}^{-1}$ , a band for the O–C–O stretching [43]. The absorption peaks at 536  $\text{cm}^{-1}$  and 694  $\text{cm}^{-1}$  could be related to the Fe–O vibration and the other peaks at 472  $\text{cm}^{-1}$  and 797  $\text{cm}^{-1}$  pure maghemite [44]. However, maghemite was not detected in the XRD pattern, likely due to its trace amount, which was less than the detection

level of the used equipment. As shown in Figure 2, the XRD pattern of the nanocomposite produced also confirms the formation of magnetite. The quantities of the phases in the nanocomposite are given in Table 3, indicating the magnetite in the composite. The TEM analysis evaluated the size and shape of the magnetite

particles produced in the composite. As seen in Figure 4, the approximately spherical shape of magnetite nanoparticles can be observed in the TEM image. Visual analysis of the TEM image using the ImageJ® software showed that the synthesized magnetite nanoparticles had a mean size of about 10.12 nm.

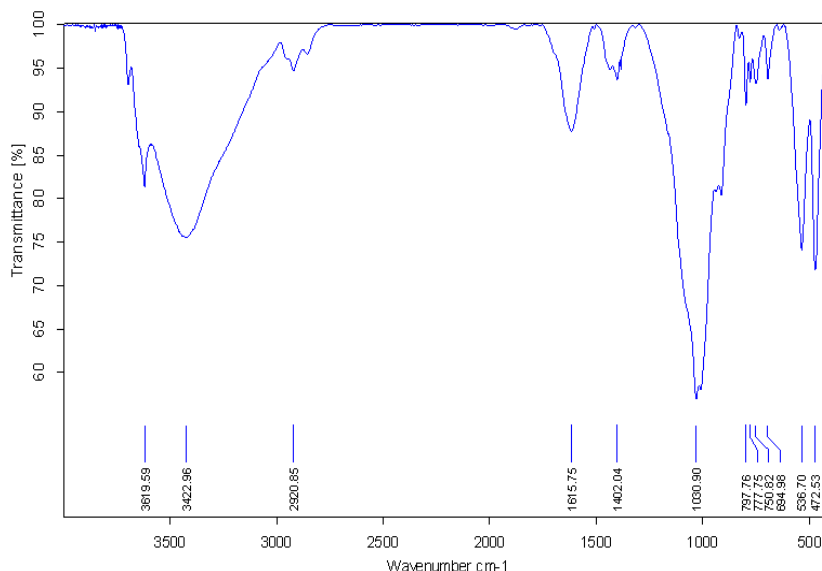


Figure 3. FT-IR spectrum of nanocomposite performed by 200 mg KBr.

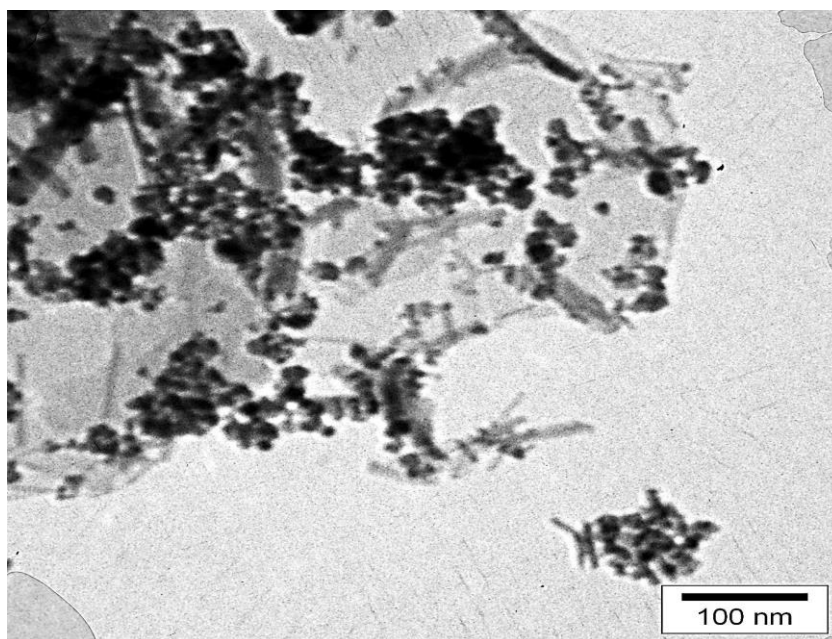


Figure 4. TEM image of synthesized nanocomposite at 160,000× magnification.

### 3.2. Statistical analysis of experimental design

The response space of the process is modelled in the central composite designs using a non-linear quadratic regression equation to predict the relationship between the operating variables and

the process responses. The general structure of this prediction model is as follows [45]:

$$y = b_0 + \sum b_i x_i + \sum b_{ij} x_i x_j + \varepsilon \tag{2}$$

where  $y$  is the predicted response,  $b$  values are the state coefficients with representative indices of 0,  $i$  and  $ij$  corresponding to constant, linear and

non-linear values. The coded values of the independent process variables are indicated by  $x_i$  and  $x_j$ . The residual error is designated by  $\varepsilon$ . The state coefficients for the process space of this work was calculated using Stat-Ease Design-Expert v.7 (DX7) and the following equation was found to be the best fitted prediction model:

$$\begin{aligned} \text{Cd Removal (\%)} = & 56.06 + 24.81 \times \text{pH} + 11.83 \\ & \times \text{F/M} - 3.41 \times \text{pH} \times \text{F/M} \\ & + 7.31 \times \text{pH}^2 \end{aligned} \quad (3)$$

The above equation was then employed to evaluate the effect of the operating variables on the adsorption efficiency. The significance of the prediction model and effects, both primary and interaction, were determined using Analysis of

Variance (ANOVA) within a confidence interval of 95%. The ANOVA results are presented in Table 4, which clearly show that the developed model is highly significant with a deficient  $p$  model (probability value  $< 0.0001$ ) and high value of  $F$  model (Fisher's  $F$ -test = 52.65). Moreover, the ANOVA results reveal that the effects of both of the operating variables are significant due to their probability values being less than 0.05. Although the interaction between the variables (AB) is not substantial, it had a significant role in the accuracy of the prediction model as recognized during the model modification stage. The model accuracy coefficients with and without AB factor are compared in Table 5.

**Table 4. Significance of prediction model and effects of variables based on ANOVA results.**

Source	Sum of Squares	df	Mean Square	F Value	p-value Prob > F	
Model	12149.23	4	3037.307	52.64769	< 0.0001	significant
A-pH	8356.162	1	8356.162	144.843	< 0.0001	
B-F/M ratio	2239.862	1	2239.862	38.82504	< 0.0001	
AB	92.88845	1	92.88845	1.610098	0.2226	
A <sup>2</sup>	556.9529	1	556.9529	9.654039	0.0068	
Residual	923.0588	16	57.69118			
Lack-of-fit	879.3596	4	219.8399	60.36892	< 0.0001	significant
Pure Error	43.69928	12	3.641607			
Cor Total	13072.29	20				

**Table 5. Comparison between accuracy coefficients for RSM model with and without AB factor.**

Model	R-Squared	Adj R-Squared	Pred R-Squared	Adeq Precision
AB included	0.9294	0.9117	0.8638	22.2488
AB removed	0.8840	0.8706	0.8123	16.2111

The significance of the developed prediction model can also be assessed using the residuals normal probability plot (NP) provided that a relatively uniform trend with no far-points is observed [46]. The Cd removal NP presented in Figure 5(a) confirms the normality assumption and significance of model Eq(3). Other pieces of evidence of the high accuracy of the prediction model are the relatively high values of the normal and adjusted correlation coefficients ( $R^2 = 92.94\%$  and  $\text{Adj } R^2 = 91.17\%$ ) that are consistent with the

model prediction accuracy plot (Figure 5(b)) with an acceptable fitting coefficient (Pred  $R^2$ ) of 86.38%. The reasonable agreement between Pred  $R^2$  and Adj  $R^2$  indicates that the model can predict the process response under new operational conditions inside the design space [47]. Another measure of the model prediction accuracy is the signal-to-noise ratio (Adeq precision), greater than 4 [39]. The Adeq precision of 22.25 indicates that model Equation (3) can be reliably used to navigate the design space.

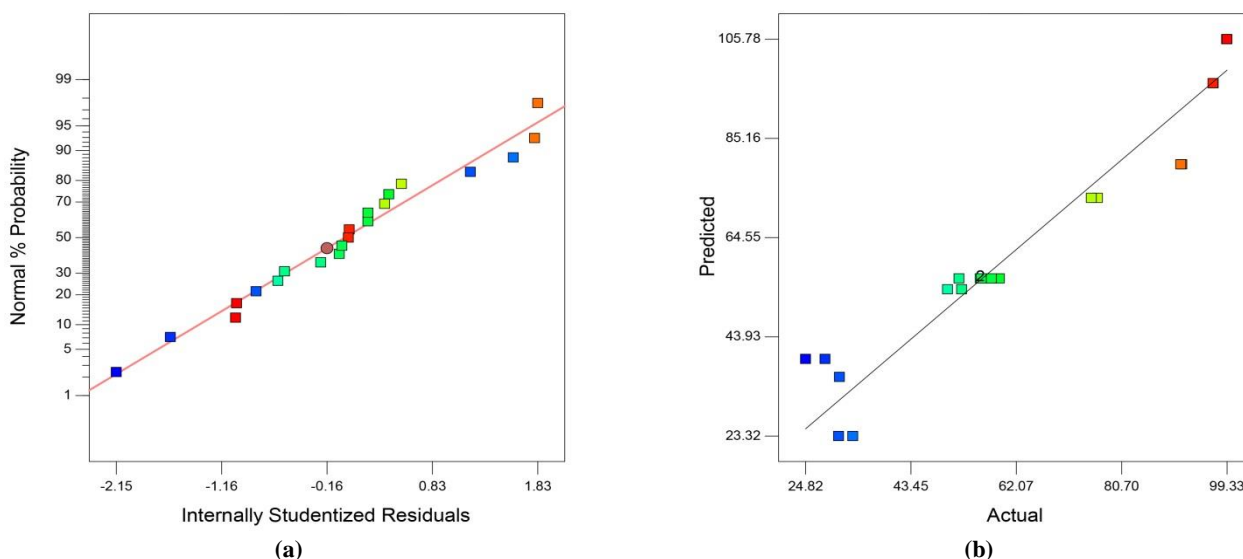


Figure 5. Residual normal plot (a) and prediction accuracy plot (b) for cadmium removal as model response.

### 3.3. Effects of variables on adsorption efficiency

Main effect plots are useful tools to monitor the pure effects of operating variables on the process response. These plots include a continuous line confined to two experimental points measured during the experimental works. For each factor, points constructing the continuous line section are calculated by the prediction model (Equation (3)), while other factors are kept constant at their mid-levels. The main plots may appear either as a straight line or as a curve in the absence or presence of a non-linear effect, respectively. Figure 6 shows the selected operating variables that influence the efficiency of Cd adsorption.

The variation of Cd adsorption at different solution pHs is shown in Figure 6(a). As shown, the Cd adsorption efficiency grows increased as the initial solution pH. The pH value of the aqueous solution has significant effects on both the adsorption process and the capacity of the coal waste. It is shown that the point of zero charges (PZC) of coal materials varies in the pH range of 6-6.5 depending on the ash content of the coal

sample [48, 49]. Moreover, PZC of magnetite was around 6.5 [50], and the surface of the nanocomposite particles became negatively charged at pH values higher than PZC. Therefore, the increase of cadmium adsorption at alkaline pH can be attributed to the higher active points of nanocomposite particles, which increases the Cd cation adsorption through electrostatic forces of attraction and provides multi-layer adsorption. The solution pH can also influence the degree of speciation and ionization of the aqueous adsorbate species. It has been demonstrated that at pH values over 7, cadmium tends to form hydroxide components [51]. Therefore, the cadmium precipitation in Cd (OH)<sub>2</sub> can be another reason behind the enhanced removal of Cd in alkaline environments. The effect of nanocomposite dosage on Cd removal is presented in Figure 6(b). Generally, increasing the adsorbent dosage improves Cd removal by providing more adsorption sites in the process environment. As a consequence, more cation species can adsorb on the nanocomposite surface.

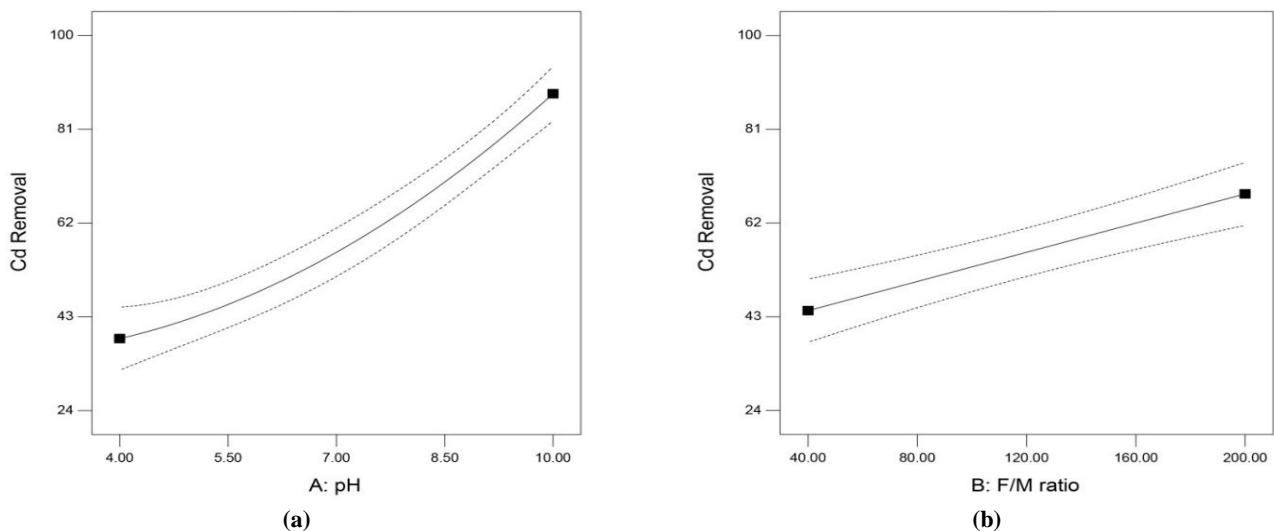


**Figure 6.** Effect of operating variables on efficiency of cadmium adsorption: (a) initial solution pH and (b) nanocomposite to Cd ratio.

### 3.4. Interaction effect and process optimization

The interactive relationship between two independent variables can be monitored by drawing the three-dimensional (3D) surface plots on which the variations of process response are predicted using the model equation proposed by the experimental design. Similar to main effect plots, those variables not considered in the 3D interaction plots are maintained at their mid-levels [52]. These 3D plots are a useful tool for evaluating the interaction effect and helpful in gaining a rough estimation of the optimal conditions under which the minimum/maximum value of the target response can be obtained. For this purpose, the interaction 3D surface plot is visualized in Figure 7, indicating that maximum Cd removal may be achieved for the initial solution pH and nanocomposite/Cd ratio at their upper levels.

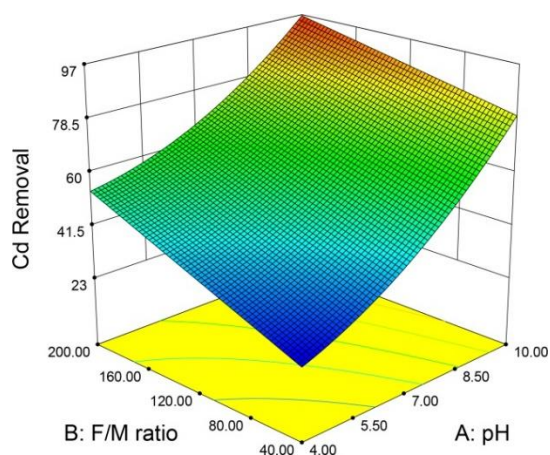


**Figure 7.** 3D response plot visualizing interaction between operating variables on Cd adsorption.

One of the functional abilities of the Design-Expert software is to propose optimum levels for the operating variables at which the most desirable process response(s) may be obtained. The software utilizes a series of numerical calculations to extract a list of optimum operating conditions with their corresponding process response(s) based on the prediction model (Equation (3) in this study). Therefore, DX7 suggested four optimal conditions sets with maximum Cd removal of almost 100% after setting the variation domain of each model variable (Table 6). The suggested optimal conditions were practically validated using adsorption experiments. The results are shown in Table 6, according to which the suggested condition No. 4 would be the best choice due to significantly lower nanocomposite consumption.

In order to attain a more precise perspective on the influence of nanoparticle loading on enhancing the absorption capacity of coal waste, an auxiliary adsorption experiment was also performed using raw coal waste at optimum operating conditions. The low average Cd removal of 43.72% was obtained after thrice replications. There are two solutions to compensate for the low adsorptive capacity of raw coal waste, i.e. increasing the dosage of adsorbent and/or prolonging the contact time. However, both of them may lead to some technical and cost limits. Therefore, the promising efficacy of the  $F_3O_4@$ coal waste nanocomposite can be verified as such.

**Table 6. Optimum levels for operating variables proposed by DX7 for maximum Cd adsorption.**

Set No.	pH	F/M Ratio	Predicted removal (%)	Prediction desirability	Experimental removal (%)
1	10.57	161.40	100	1.00	99.49
2	10.83	123.27	99.99	1.00	99.51
3	10.54	166.13	99.99	1.00	99.13
4	11.04	89.72	100	1.00	99.24

### 3.5. Adsorption kinetics

Generally, the kinetics of any adsorption process can be investigated using the pseudo first-order model:

$$\ln\left(1 - \frac{q_t}{q_e}\right) = -k_1 t \quad (4)$$

where  $k_1$  is the rate constant ( $\text{h}^{-1}$ ) and  $q_e$  ( $\text{mg/g}$ ) is the equilibrium amount of solute adsorbed on the adsorbent surface; and the pseudo second-order model [53]:

$$\frac{1}{q_t} - \frac{1}{q_e} = \frac{1}{k_2 q_e^2 t} \quad (5)$$

where  $k_2$  is the rate constant under equilibrium conditions ( $\text{g.mg}^{-1} \text{h}$ ), the amount of solute adsorbed at any time  $t$  ( $q_t$ ,  $\text{g.mg}^{-1}$ ) is calculated as below:

$$q_t = \frac{(C_0 - C_t)V}{W} \quad (6)$$

where  $C_0$  and  $C_t$  are the initial and the liquid-phase concentrations of Cd at time  $t$  ( $\text{mg/L}$ ), respectively. The variables  $W$  ( $\text{g}$ ) and  $V$  ( $\text{L}$ ) designate the adsorbent mass and solution volume. The results of fitting kinetic data to the pseudo-first and -second-order models for Cd adsorption on nanocomposite are illustrated in Figure 8.

As shown in Figures 8(a) and 8(b), the adsorption process does not show an acceptable agreement with any of the kinetic models. However, the correlation coefficient for the pseudo-first-order model is much higher than the pseudo-second-order model. For this reason, the data was also matched to the classical first-order kinetic model to assess the process compatibility with first-order absorption [54]:

$$R = R_\infty(1 - e^{-kt}) \quad (7)$$

in which  $R_\infty$  is the maximum achievable removal (%), and  $k$  is the rate constant ( $1/\text{h}$ ). The results of fitting the adsorption data with Equation (7) are shown in Figure 8(c). As shown, the

adsorption process follows first-order kinetics with very high accuracy levels. The remarkable point about this chart is the considerable absorption rate so that the maximum absorption is achieved in less than a minute (scaled-up chart). These results indicate that the nanocomposite produced has a remarkable ability to rapidly treat aqueous environments contaminated with heavy metals.

### 3.6. Adsorption isotherms

One of the critical aspects of any adsorption process is the interaction mechanism of the adsorbate with the surface of the adsorbent under given conditions, i.e. equilibrium states and constant temperatures. Such studies are conducted by developing the equilibrium isotherm plots. Among numerous isotherm models, the Langmuir, Freundlich, Temkin, and Jovanoic ones have been widely employed by many researchers. Each one of these models can open up the potential phenomena behind the adsorption of a pollutant on a particular adsorbent. The Langmuir isotherm, for example, is the indicator of homogenous monolayer adsorption of cations/anions on the adsorbent surface over a uniform distribution of adsorption energies [55–57]. The multi-layer adsorption mechanism can be recognized by the Freundlich isotherm model with non-uniform energy distribution [53, 58]. The Temkin isotherm is another interesting model describing the linear dwindling of adsorption heat of the layer of pollutant molecules adsorbed. However, the common aspect of this model with Langmuir is the uniform distribution of binding energy but up to a maximum level [57]. The Jovanoic isotherm is likely a more similar model to Langmuir in assumptions considering possible mechanical interactions among the species, which adsorb and/or desorb over the surface of the adsorbent [59]. The general formula of the isotherm mentioned above models with corresponding parameters is listed in Table 7.

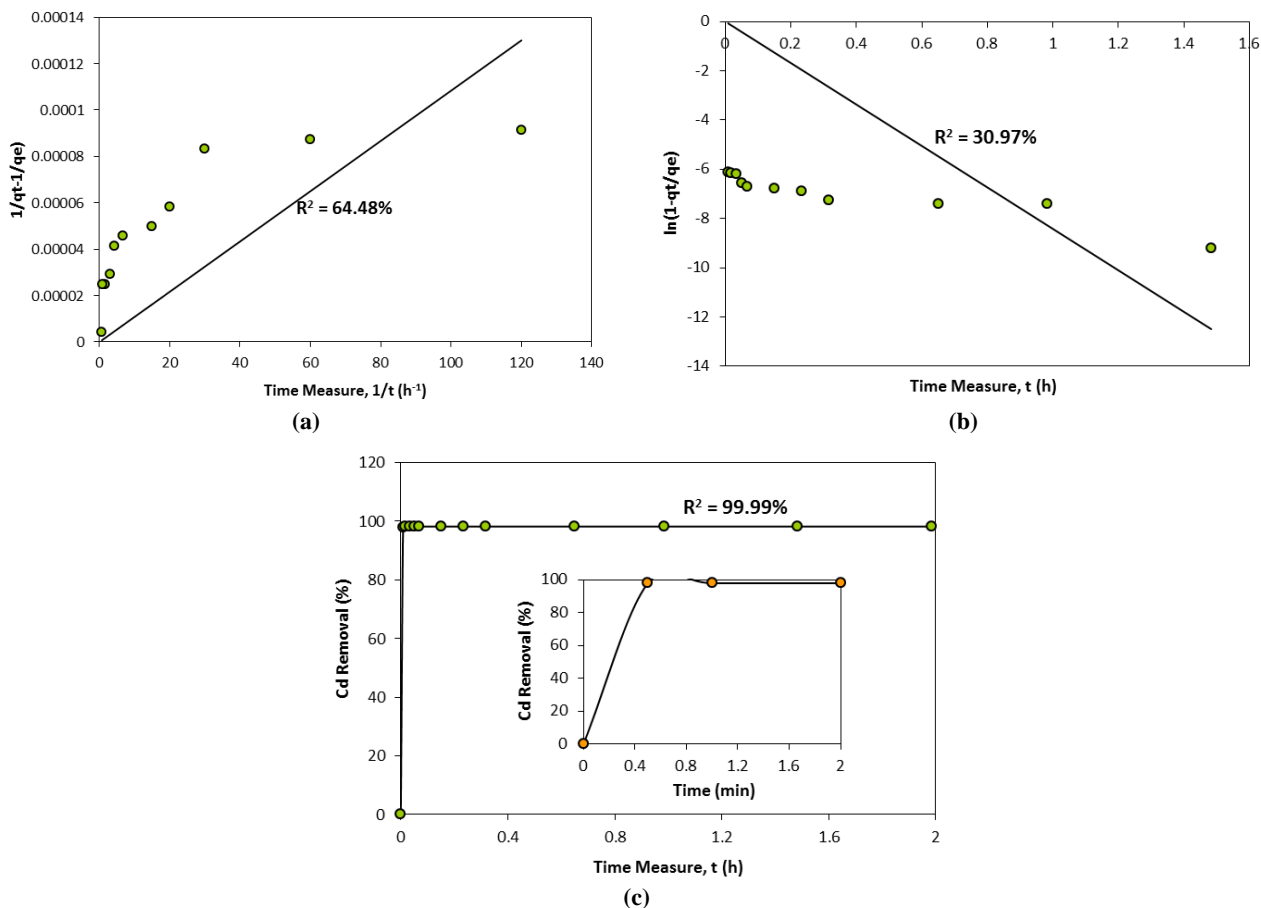


Figure 8. Kinetic model plots for pseudo-first-order (a), pseudo-second-order (b), and classic first-order kinetic models of cadmium adsorption.

Table 7. General and linearized forms of the studied isotherm models as well as their fitting parameters.

Isotherm type	Langmuir	Freundlich	Temkin	Jovanoic
Model equation	$q_e = \frac{q_m K_L C_e}{1 + K_L C_e}$	$q_e = K_L C_e^{1/n}$	$q_e = q_m \ln(K_T C_e)$	$q_e = q_m \exp(K_J C_e)$
Linear expression	$\frac{q_e}{C_e} = \left( \frac{1}{K_L q_m} \right) + \left( \frac{C_e}{q_m} \right)$	$\ln q_e = \ln K_F + \frac{1}{n} \ln C_e$	$q_e = q_m \ln K_T + q_m \ln C_e$	$\ln q_e = \ln q_m + K_J C_e$
Plot axis	$\frac{q_e}{C_e}$ vs. $C_e$	$\ln q_e$ vs. $\ln C_e$	$q_e$ vs. $\ln C_e$	$\ln q_e$ vs. $C_e$
Parameters	$q_m = (\text{slope})^{-1}$ , $K_L = \text{slope/intercept}$	$K_F = \exp(\text{intercept})$ , $n = (\text{slope})^{-1}$	$K_T = \exp(\text{intercept/slope})$ , $q_m = \text{slope}$	$q_m = \exp(\text{intercept})$ , $K_J = \text{slope}$

Each model should be first fitted with the experimental data to find the model parameters to assess the compatibility of models with adsorption results (Figure 9). The fitting is conducted using numerical solvation to reach the least square error. The applicability of models is then evaluated by the values of correlation coefficient ( $R^2$  values) and average relative error (ARE) as follows [60]:

$$ARE = \frac{100}{N} \sum_{i=1}^N \left| \frac{q_{e,exp} - q_{e,cal}}{q_{e,exp}} \right| \tag{8}$$

Where the indices exp and cal designate the experimental and calculated equilibrium concentrations of cadmium, respectively. The number of experiments is indicated as  $N$ .

Generally, the best-fit model is recognized by its lowest ARE and highest  $R^2$  values. Table 8 lists the fitting results for the selected isotherm models and their applicability measures. The fitting measures indicate that the Temkin isotherm model can describe the adsorption mechanism more precisely than other models, with the highest correlation coefficient (95.58%) and the lowest ARE (25.88%).

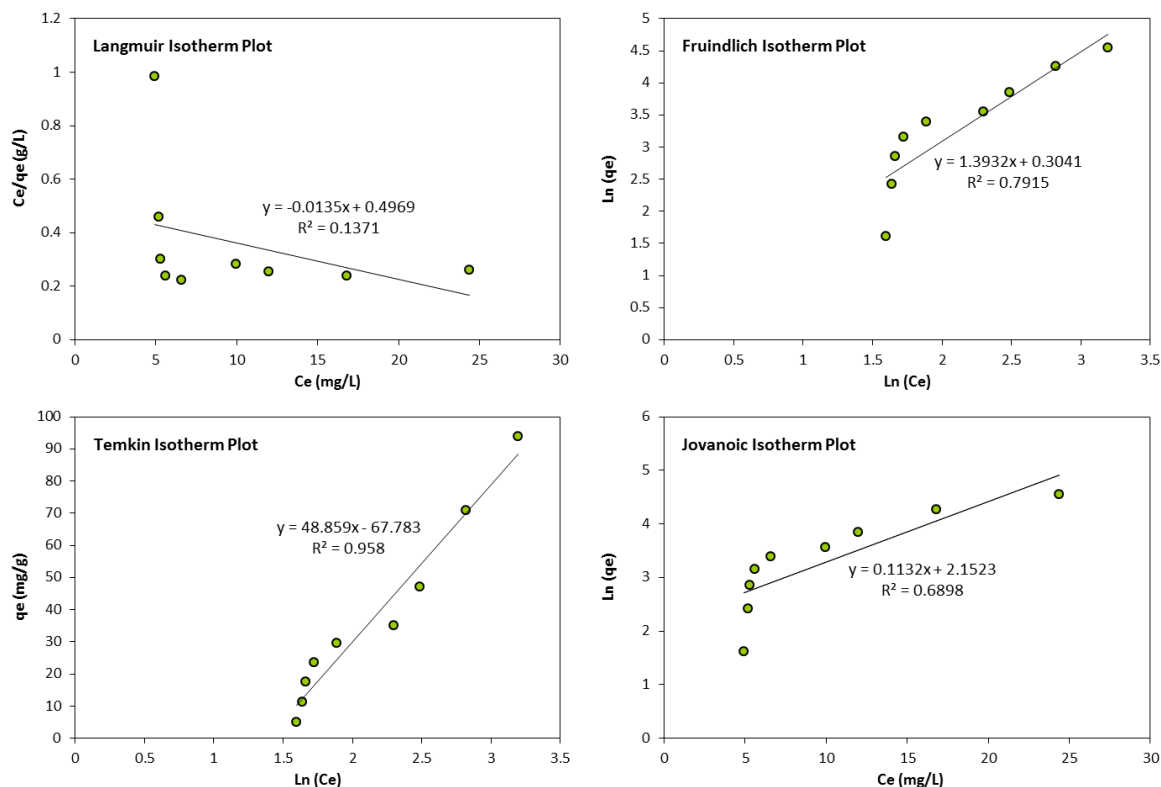


Figure 9. Illustration of isotherm models for Cd adsorption onto nanocomposite.

Table 8. Values of model factors and fitting coefficients for Cd adsorption.

Isotherm	Model parameters		Correlation coefficient ( $R^2$ , %)	Relative error (ARE, %)
Langmuir	$q_m = 74.074$	$K_L = 0.027$	13.71	97.74
Freundlich	$K_F = 1.355$	$n = 0.718$	79.15	84.55
Temkin	$q_m = 48.859$	$K_T = 0.250$	95.58	25.88
Jovanoic	$q_m = 8.605$	$K_J = 0.113$	68.98	48.28

### 3.7. Proposed mechanism for cadmium removal

Generally, the following remarks can be denoted from the previous sections:

- Cadmium removal was directly influenced from the solution pH and improved as the pH was increased (Figure 6a).
- Optimal pH to achieve maximum removal was found to be around 11 (Table 5).
- Cadmium ions begin to precipitate at alkaline pH values [61].
- Non-linear trends were observed in both the kinetics and isotherm plots (Figure 8c and 9).

This information implies that there might be a multi-step process responsible for Cd removal from aqueous solution. In order to explore the potential mechanism(s) involved in the removal process, the behavior of adsorption was analyzed based on the Weber and Morris equation or

intraparticle diffusion model (IPD) shown in the Equation (9) [62]:

$$q_t = k_{IPD} t^{0.5} + C \quad (9)$$

where  $k_{IPD}$  (mg/g.min<sup>1/2</sup>) and  $C$  (mg/g) are the model parameters. These constants are obtained by fitting the  $q_t$  versus  $t^{0.5}$  using the least square error solving technique. It should be noted that the fitting process includes multiple steps to achieve the best compatibility between experimental and calculation results. The fitting plot is illustrated in Figure 10 showing that the Cd removal follows a two-step process. The IPD constants presented in Table 9 reveal that the removal follows a fast process from the earliest adsorption to 4 min (2 min<sup>1/2</sup>) of contact time and then significantly slow down to the end of the removal process ( $K_1 \gg K_2$ ). The structure of the IPD model is also in agreement with the first-order kinetics results shown in Figure 8c.

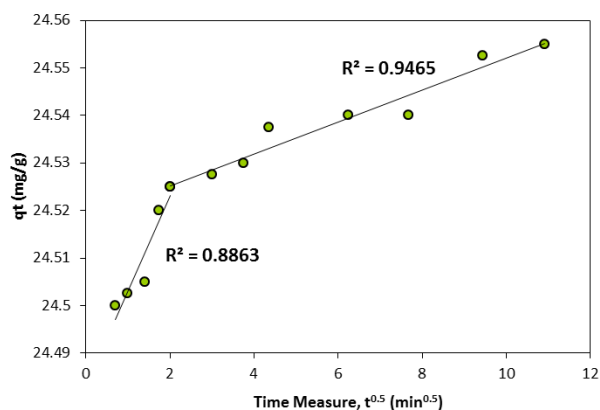


**Figure 10.** Illustration of intraparticle diffusion model for Cd removal.

**Table 9.** Parameters of the intraparticle diffusion model for Cd removal.

Step	$k_{IPD}$ ( $\text{mg/g}\cdot\text{min}^{1/2}$ )	$C$ (mg/g)	$R^2$ (%)
First	0.020	24.483	88.63
Second	0.003	24.519	94.65

The increasing dependency of removal efficiency to solution pH (Figure 6a) indicates that a combination of adsorption and precipitation mechanisms may be responsible for the final removal of Cd from aqueous solution using the  $\text{Fe}_3\text{O}_4@\text{CW}$  nanocomposite. Therefore, the first

section in Figure 10 can be attributed to adsorption (monolayer coverage), while the second phase indicates a different reaction occurring on the surface, most likely surface precipitation. However, the transition between the two reactions is not apparent in the adsorption isotherms. The proposed removal mechanism is schematically illustrated in Figure 11. Up to the contact time of 4 min, a rapid first adsorption stage based on the Temkin mechanism with surface or film diffusion from the cadmium bulk solution to  $\text{Fe}_3\text{O}_4$  nanoparticles on the surface of coal waste occurs [63]. The peak of this step can be observed in the first minute of the process as observed in both the kinetics (Figure 8c) and IPD (Figure 10) plots. Then the active sites on the surface of  $\text{Fe}_3\text{O}_4$  nanoparticles and likely coal waste particles tend to become saturated after about 4 min. In the second stage, cadmium precipitates in the form of hydroxide settle down on the surface of nanocomposite and occupy the pores between  $\text{Fe}_3\text{O}_4$  nanoparticles at the surface of coal waste. The same mechanism has also been suggested by Li and Stanforth [64], who showed that such multi-step adsorption/precipitation processes may be occurring in some of the adsorption studies, particularly at high pH values.

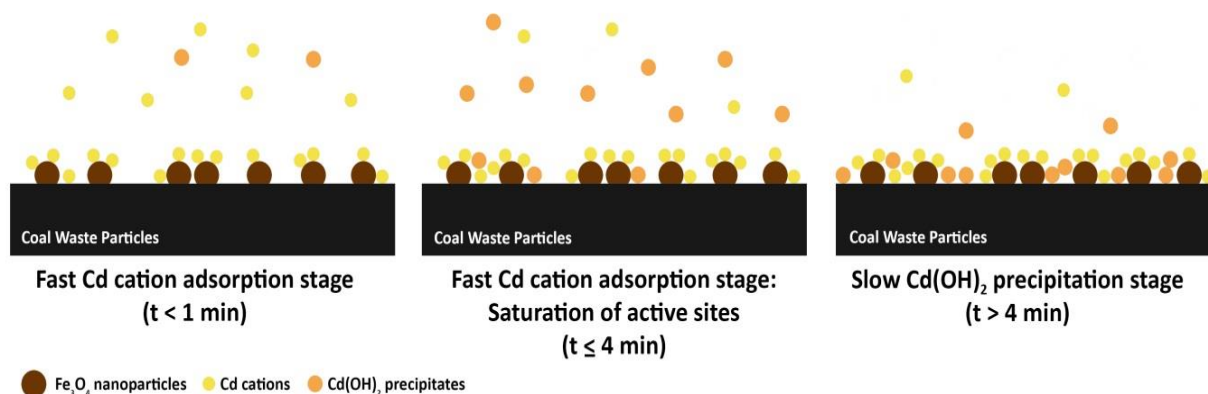


**Figure 11.** A simple illustration of two-step Cd removal using  $\text{Fe}_3\text{O}_4@\text{CW}$  nanocomposite.

#### 4. Conclusions

A nanocomposite adsorbent synthesized based on  $\text{Fe}_3\text{O}_4$  nanoparticles, and coal waste (CW) was employed to eliminate the Cd (II) ions from an aquatic environment. The overall adsorption capacity was 48.86 mg/g using batch tests arranged using the CCD experimental design. The significant Cd removal was over 99% using absorbent to adsorbate ratio of 90 and solution pH of 11. Characterization of the  $\text{Fe}_3\text{O}_4@\text{CW}$  nanocomposite was made using the FT-IR

spectroscopy, XRD, and TEM analyses. The adsorption process was best suited to the Temkin isothermal model for the experimental results. Moreover, the cadmium adsorption process was perfectly matched to the classic first-order kinetic model on the surface of the  $\text{Fe}_3\text{O}_4@\text{CW}$  nanocomposite. The removal was described by a two-stage intraparticle diffusion model in which the Cd removal in the initial stage was fast via adsorption, and then a second slower precipitation stage took place. However, further experimental and analytical investigations may be suggested to

explore the actual mechanisms behind the adsorption process. This study demonstrated that the  $\text{Fe}_3\text{O}_4@\text{CW}$  nanocomposite could be considered an efficient adsorbent for treating heavy metal-contaminated wastewater. As mentioned earlier, several parameters affect the absorption process, the most important of which was investigated in this work. Therefore, in order to further evaluate, it is recommended to study other variables such as stirring speed, temperature, competitive effect of other cations, and solution hardness.

## References

- [1]. Shojaei, V. and Khoshdast, H. (2018). Efficient chromium removal from aqueous solutions by precipitate flotation using rhamnolipid biosurfactants. *Physicochemical Problems of Mineral Processing*, 54 (3): 1014–1025.
- [2]. Bodagh, A., Khoshdast, H., Sharafi, H., Zahiri, H.S. and Akbari Noghabi, K. (2013). Removal of cadmium (II) from aqueous solution by ion flotation using rhamnolipid biosurfactant as ion collector. *Industrial and Engineering Chemistry Research*. 52 (10): 3910–3917.
- [3]. Shami, R.B., Shojaei, V. and Khoshdast, H. (2019). Efficient cadmium removal from aqueous solutions using a sample coal waste activated by rhamnolipid biosurfactant. *Journal of Environmental Management*, 231: 1182–1192.
- [4]. Wei, J., Tu, C., Yuan, G., Bi, D., Xiao, L., Theng, B.K.G., Wang, H. and Ok, Y.S. (2019). Carbon-coated montmorillonite nanocomposite for the removal of chromium (VI) from aqueous solutions. *Journal of Hazardous Materials*, 368: 541–549.
- [5]. Singh, N.B. and Rachna, K.M. (2020). Copper ferrite-Polyaniline nanocomposite and its application for Cr (VI) ion removal from aqueous solution. *Environmental Nanotechnology, Monitoring and Management*, 14, 100301.
- [6]. Dinh, V.P., Nguyen, M.D., Nguyen, Q.H., Do, T.T.T., Luu, T.T., Luu, A.T., Tap, T.D., Ho, T.H., Phan, T.P., Nguyen, T.D. and Tan, L.V. (2020). Chitosan-MnO<sub>2</sub> nanocomposite for effective removal of Cr (VI) from aqueous solution. *Chemosphere*, 257, 127147.
- [7]. Zhang, C., Luan, J., Yu, X. and Chen, W. (2019). Characterization and adsorption performance of graphene oxide–montmorillonite nanocomposite for the simultaneous removal of  $\text{Pb}^{2+}$  and p-nitrophenol. *Journal of Hazardous Materials*, 378, 120739.
- [8]. Irandoost, M., Pezeshki-Modaress, M. and Javanbakht, V. (2019). Removal of lead from aqueous solution with nanofibrous nanocomposite of polycaprolactone adsorbent modified by nanoclay and nanozeolite. *Journal of Water Process Engineering*, 32, 100981.
- [9]. Akbarzadeh, M.J., Hashemian, S. and Mokhtarian, N. (2020). Study of Pb(II) removal ZIF@NiTiO<sub>3</sub> nanocomposite from aqueous solutions. *Journal of Environmental Chemical Engineering*. 8 (2): 103703.
- [10]. Wu, Q., Wang, D., Chen, C., Peng, C., Cai, D. and Wu, Z. (2021). Fabrication of  $\text{Fe}_3\text{O}_4/\text{ZIF-8}$  nanocomposite for simultaneous removal of copper and arsenic from water/soil/swine urine. *Journal of Environmental Management*, 290, 112626.
- [11]. Jung, K.W., Lee, S.Y., Choi, J.W. and Lee, Y.J. (2019). A facile one-pot hydrothermal synthesis of hydroxyapatite/biochar nanocomposites: Adsorption behavior and mechanisms for the removal of copper (II) from aqueous media. *Chemical Engineering Journal*, 369: 529–541.
- [12]. Alhan, S., Nehra, M., Dilbaghi, N., Singhal, N.K., Kim, K.H. and Kumar, S. (2019). Potential use of ZnO@activated carbon nanocomposites for the adsorptive removal of  $\text{Cd}^{2+}$  ions in aqueous solutions. *Environmental Research*, 173: 411–418.
- [13]. Chen, H., Zhang, Z., Zhong, X., Zhuo, Z., Tian, S., Fu, S., Chen, Y. and Liu, Y. (2021). Constructing MoS<sub>2</sub>/Lignin-derived carbon nanocomposites for highly efficient removal of Cr (VI) from aqueous environment. *Journal of Hazardous Materials*, 408, 124847.
- [14]. Gupta, V.K. and Nayak, A. (2021). Cadmium removal and recovery from aqueous solutions by novel adsorbents prepared from orange peel and  $\text{Fe}_2\text{O}_3$  nanoparticles. *Chemical Engineering Journal*, 180: 81–90.
- [15]. Gong, J., Chen, L., Zeng, G., Long, F., Deng, J., Niu, Q. and He, X. (2012). Shellac-coated iron oxide nanoparticles for removal of cadmium (II) ions from aqueous solution. *Journal of Environmental Sciences*. 24 (7): 1165–1173.
- [16]. Abd El-Latif, M.M., Ibrahim, A.M., Showman, M.S. and Abdel Hamide, R.R. (2013). Alumina/iron oxide nanocomposite for cadmium ions removal from aqueous solutions. *International Journal of Nonferrous Metallurgy*, 2 (2): 47–62.
- [17]. Banerjee, S., Kumar, N.P., Srinivas, A. and Roy, S. (2019). Core-shell  $\text{Fe}_3\text{O}_4@\text{Au}$  nanocomposite as dual-functional optical probe and potential removal system for arsenic (III) from Water. *Journal of Hazardous Materials*, 375: 216–223.
- [18]. Eslami, H., Esmaili, A., Ehrampoush, M.H., Ebrahimi, A.A., Taghavi, M. and Khosravi, R. (2020). Simultaneous presence of poly titanium chloride and  $\text{Fe}_2\text{O}_3\text{-Mn}_2\text{O}_3$  nanocomposite in the enhanced coagulation for high rate As (V) removal from contaminated water. *Journal of Water Process Engineering*, 36, 101342.

- [19]. Zeng, X., Wang, Y., He, X., Liu, C., Wang, X. and Wang, X. (2021). Enhanced removal of Cr (VI) by reductive sorption with surface-modified  $Ti_3C_2T_x$  MXene nanocomposites. *Journal of Environmental Chemical Engineering*, 9 (5): 106203.
- [20]. Peighambardoust, S.J., Foroutan, R., Peighambardoust, S.H., Khatooni, H. and Ramavandi, B. (2021). Decoration of Citrus limon wood carbon with  $Fe_3O_4$  to enhanced  $Cd^{2+}$  removal: A reclaimable and magnetic nanocomposite. *Chemosphere*, 282, 131088.
- [21]. Priyan, V.V., Kumar, N. and Narayanasamy, S. (2021). Development of  $Fe_3O_4/CAC$  nanocomposite for the effective removal of contaminants of emerging concerns ( $Ce^{3+}$ ) from water: An ecotoxicological assessment. *Environmental Pollution*, 285, 117326.
- [22]. Ghorbani, F., Kamari, S., Askari, F., Molavi, H. and Fathi, S. (2021). Production of nZVI-Cl nanocomposite as a novel eco-friendly adsorbent for efficient As (V) ions removal from aqueous media: Adsorption modelling by response surface methodology. *Sustainable Chemistry and Pharmacy*, 21, 100437.
- [23]. Sharma, A., Singh, M., Arora, K., Singh, P.P., Badru, R., Kang, T.S. and Kaushal, S. (2021). Preparation of cellulose acetate-Sn (IV) iodophosphate nanocomposite for efficient and selective removal of  $Hg^{2+}$  and  $Mn^{2+}$  ions from aqueous solution. *Environmental Nanotechnology, Monitoring and Management*, 16, 100478.
- [24]. Usman, M., Ahmed, A., Ji, Z., Yu, B., Shen, Y. and Cong, H. (2021). Environmentally friendly fabrication of new  $\beta$ -Cyclodextrin/ $ZrO_2$  nanocomposite for simultaneous removal of Pb (II) and BPA from water. *Science of the Total Environment*, 784, 147207.
- [25]. Narayana, P.L., Lingamdinne, L.P., Karri, R.R., Devanesan, S., Al Salhi, M.S., Reddy, N.S., Chang, Y.Y. and Koduru, J.R. (2022). Predictive capability evaluation and optimization of Pb(II) removal by reduced graphene oxide-based inverse spinel nickel ferrite nanocomposite. *Environmental Research*, 204, 112029.
- [26]. Ghaeni, N., Taleshi, M.S. and Elmi, F. (2019). Removal and recovery of strontium (Sr(II)) from seawater by  $Fe_3O_4/MnO_2$ /fulvic acid nanocomposite. *Marine Chemistry*, 213: 33–39.
- [27]. Li, Z., Pan, Z. and Wang, Y. (2020). Mechanochemical preparation of ternary polyethyleneimine modified magnetic illite/smectite nanocomposite for removal of Cr (VI) in aqueous solution. *Applied Clay Science*, 198, 105832.
- [28]. Reis, E.D.S., Gorza, F.D.S., Pedro, G.D.C., Maciel, B.G., Silva, R.J.D., Ratkovski, G.P. and Melo, C.P.D. (2021). (Maghemite/Chitosan/Polypyrrole) nanocomposites for the efficient removal of Cr (VI) from aqueous media, *Journal of Environmental Chemical Engineering*. 9 (1): 104893.
- [29]. Sarojini, G., Venkateshbabu, S. and Rajasimman, M. (2021). Facile synthesis and characterization of polypyrrole – iron oxide – seaweed (PPy- $Fe_3O_4$ -SW) nanocomposite and its exploration for adsorptive removal of Pb(II) from heavy metal bearing water. *Chemosphere*, 278, 130400.
- [30]. Verma, M., Lee, I., Oh, J., Kumar, V. and Kim, H. (2022). Synthesis of EDTA-functionalized graphene oxide-chitosan nanocomposite for simultaneous removal of inorganic and organic pollutants from complex wastewater. *Chemosphere*. 287 (4): 132385.
- [31]. Khalith, S.B.M., Ramalingam, R., Karuppanan, S.K., Dowlath, M.J.H., Kumar, R., Vijayalakshmi, S., Maheshwari, R.U. and Arunachalam, K.D. (2022). Synthesis and characterization of polyphenols functionalized graphitic hematite nanocomposite adsorbent from an agro waste and its application for removal of Cs from aqueous solution. *Chemosphere*. 286 (1): 131493.
- [32]. Shariatinia, Z. and Esmaeilzadeh, A. (2019). Hybrid silica aerogel nanocomposite adsorbents designed for Cd (II) removal from aqueous solution. *Water Environment Research*. 91 (12): 1624–1637.
- [33]. Xu, L., Chen, J., Wen, Y., Li, H., Ma, J. and Fu, D. (2016). Fast and effective removal of cadmium ion from water using chitosan encapsulated magnetic  $Fe_3O_4$  nanoparticles. *Desalination and Water Treatment*, 57: 8540–8548.
- [34]. Kang, A.J., Baghdadi, M. and Pardakhti, A. (2016). Removal of cadmium and lead from aqueous solutions by magnetic acid-treated activated carbon nanocomposite. *Desalination and Water Treatment*. 57 (40): 18782–18798.
- [35]. Ruthiraan, M., Abdullah, E.C., Mubarak, N.M. and Noraini, M.N. (2017). A promising route of magnetic based materials for removal of cadmium and methylene blue from waste water. *Journal of Environmental Chemical Engineering*. 5 (2): 1447–1455.
- [36]. Zubrik, A., Matik, M., Lovás, M., Danková, Z., Kaňuchová, M., Hredzák, S., Briančin, J. and Šepelák, V. (2019). Mechanochemically synthesised coal-based magnetic carbon composites for removing As (V) and Cd (II) from aqueous solutions. *Nanomaterials*. 9 (1): 100.
- [37]. Karimi, M.A. and Mehrjardi, A.H. (2010). *Nano Laboratory*, Payam Resan Publisher, Tehran, Iran.
- [38]. Subramonian, W., Wu, T.Y. and Chai, S.-P. (2015). An application of response surface methodology for optimizing coagulation process of raw industrial effluent using *Cassia obtusifolia* seed gum together with alum. *Industrial Crops and Products*, 70: 107–115.

- [39]. Montgomery, D.C. (2001). Design and Analysis of Experiments. John Wiley and Sons, New York.
- [40]. Kuhm, M. and Johnson, K. (2018). Applied Predictive Modelling, Springer, Germany.
- [41]. Shami, R.B., Shojaei, V. and Khoshdast, H. (2021). Removal of some cationic contaminants from aqueous solutions using sodium dodecyl sulfate-modified coal tailings. Iranian Journal of Chemistry and Chemical Engineering, 40(4): 1105–1120.
- [42]. Banivaheb, S., Dan, S., Hashemipour, H. and Kalantari, M. (2021). Synthesis of modified chitosan TiO<sub>2</sub> and SiO<sub>2</sub> hydrogel nanocomposites for cadmium removal. Journal of Saudi Chemical Society, 25, 101283.
- [43]. Eldeeb, T.M., El-Nemr, A., Khedr, M.H. and El-Dek, S.I. (2021). Novel bio-nanocomposite for efficient copper removal. Egyptian Journal of Aquatic Research, 47: 261–267.
- [44]. Darezereshki, E. (2010). Synthesis of maghemite ( $\gamma$ -Fe<sub>2</sub>O<sub>3</sub>) nanoparticles by wet chemical method at room temperature. Materials Letters, 64: 1471–1472.
- [45]. Hay, J.X.W., Wu, T.Y., Teh, C.Y. and Jahim, J.M. (2012). Optimized growth of Rhodobacter sphaeroides O.U.001 using response surface methodology (RSM). Journal of Scientific and Industrial Research. 71 (2): 149–154.
- [46]. Yetilmesoy, K., Demirel, S. and Vanderbei, R.J. (2009). Response surface modeling of Pb(II) removal from aqueous solution by Pistacia vera L.: Box–Behnken experimental design. Journal of Hazardous Materials, 171: 551–562.
- [47]. Shak, K.P.Y. and Wu, T.Y. (2015). Optimized use of alum together with unmodified Cassia obtusifolia seed gum as a coagulant aid in treatment of palm oil mill effluent under natural pH of wastewater. Industrial Crops and Products, 76: 1169–1178.
- [48]. Mori, S., Hara, T., Aso, K. and Okamoto, H. (1984). Zeta potential of coal fine-particles in aqueous suspension. Powder Technology, 40(1–3): 161–165.
- [49]. Fuerstenau, D.W., Rosenbaum, J.M. and You, Y.S. (1988). Electrokinetic behavior of coal. Energy Fuels, 2(3): 241–245.
- [50]. Rajput, S., Pittman Jr, C.U. and Mohan, D. (2016). Magnetic magnetite (Fe<sub>3</sub>O<sub>4</sub>) nanoparticle synthesis and applications for lead (Pb<sup>2+</sup>) and chromium (Cr<sup>6+</sup>) removal from water. Journal of Colloid and Interface Science, 468: 334–346.
- [51]. Poorbahaadini Zarandi, M., Khoshdast, H., Darezereshki, E. and Shojaei, V. (2020). Efficient cadmium removal from aqueous environments using a composite produced by coal fly ash and rhamnolipid biosurfactants. Journal of Minerals Resources Engineering, 5 (3): 107–126.
- [52]. Liu, H.L. and Chiou, Y.R. (2005). Optimal decolorization efficiency of reactive red 239 by UV/TiO<sub>2</sub> photocatalytic process coupled with response surface methodology. Chemical Engineering Journal. 112 (1–3): 173–179.
- [53]. Su, C.X.H., Teng, T.T., Alkarkhi, A.F.M. and Low, L.W. (2014). Imperata cylindrica (cogongrass) as an adsorbent for methylene blue dye removal: process optimization. Water, Air, & Soil Pollution, 225: 1–12.
- [54]. Gholami, A.R. and Khoshdast, H. (2020). Using artificial neural networks for the intelligent estimation of selectivity index and metallurgical responses of a sample coal bioflotation by rhamnolipid biosurfactants. Energy Sources A: Recovery, Utilization, and Environmental Effects, 1857477.
- [55]. El Nemr, A. (2009). Potential of pomegranate husk carbon for Cr (VI) removal from wastewater: kinetic and isotherm studies. Journal of Hazardous Materials, 161: 132–141.
- [56]. Sreejalekshmi, K.G., Anoopkrishnan, K. and Anirudhan, T.S. (2009). Adsorption of Pb (II) and Pb (II)-citric acid on sawdust activated carbon: kinetic and equilibrium isotherm studies. Journal of Hazardous Materials, 161: 1506–1513.
- [57]. Jalayeri, H., Salarirad, M.M. and Ziari, M. (2016). Kinetics and isotherm modelling of Zn (II) ions adsorption onto mine soils. Physicochemical Problems of Mineral Processing, 52(2): 767–779.
- [58]. Irannajad, M., Haghghi, H.K. and Soleimanipour, M. (2016). Adsorption of Zn<sup>2+</sup>, Cd<sup>2+</sup> and Cu<sup>2+</sup> on zeolites coated by manganese and iron oxides. Physicochemical Problems of Mineral Processing. 52 (2): 894–908.
- [59]. Ghosh, R.K. and Reddy, D.D. (2013). Tobacco stem ash as an adsorbent for removal of methylene blue from aqueous solution: equilibrium, kinetics, and mechanism of adsorption. Water, Air, & Soil Pollution, 224, 1–12.
- [60]. Gholami, A.R., Khoshdast, H., and Hassanzadeh, A. (2021). Applying hybrid genetic and artificial bee colony algorithms to simulate a bio-treatment of synthetic dye-polluted wastewater using a rhamnolipid biosurfactant. Journal of Environmental Management, 299, 113666.
- [61]. Luo, J., Hein, C., Müucklich, F., and Solioz, M., Killing of bacteria by copper, cadmium, and silver surfaces reveals relevant physicochemical parameters. Biointerphases. 12 (2): 1–6.
- [62]. Wu, F.C., Tseng, R.L., and Juang, R.S. (2009). Initial behaviour of intraparticle diffusion model used in the description of adsorption kinetics. Chemical Engineering Journal, 153: 1–8.
- [63]. Lopez-Luna, J., Ramirez-Montes, L.E., Martinez-Vargas, S., Martinez, A.I., Mijangos-Ricardez, O.F., Gonzalez-Chavez, M.C.A., Carrillo-Gonzalez, R.,

Solis-Dominguez, F.A., Cuevas-Diaz, M.C. and Vazquez-Hipolito, V. (2019). Linear and nonlinear kinetic and isotherm adsorption models for arsenic removal by manganese ferrite nanoparticles. *Applied Sciences*, 1, 950.

[64]. Li, L. and Stanforth, R. (2000). Distinguishing adsorption and surface precipitation of phosphate on goethite ( $\alpha$ -FeOOH). *Journal of Colloid and Interface Science*, 230: 12–21.

## مطالعه قابلیت حذف جذبی کادمیوم از محیط آبی با استفاده از باطله زغال پوشیده شده با نانوذرات $Fe_3O_4$

ساسان میرشکاری، وحیده شجاعی\* و حمید خوشدست

بخش مهندسی معدن، مجتمع آموزش عالی زرنند، زرنند، ایران

ارسال ۲۰۲۲/۰۴/۱۹، پذیرش ۲۰۲۲/۰۶/۰۸

\* نویسنده مسئول مکاتبات: v.shojaei@uk.ac.ir

### چکیده:

در این پژوهش، یک نمونه باطله زغال پوشیده شده با نانوذرات  $Fe_3O_4$  به عنوان جاذبی کارآمد جهت حذف کادمیوم از پسابی مصنوعی مورد استفاده قرار گرفت. نانوکامپوزیت تولید شده با استفاده از روشهای اسپکترومتری مادون قرمز تبدیل فوریه (FTIR)، پراش اشعه ایکس (XRD) و میکروسکوپ الکترونی روبشی (TEM) مشخصه‌یابی شد. آنالیز تصاویر میکروسکوپی نشان داد که متوسط ابعاد نانوذرات مگنتیت حدود ۱۰ نانومتر بود. تأثیر متغیرهای عملیاتی شامل pH اولیه محلول (۳-۱۱) و نسبت نانوکامپوزیت به آلاینده (۷-۲۳۳) بر جذب کادمیوم با استفاده از روش طراحی آزمایش پاسخ سطح ارزیابی شد. همچنین، فرایند جذب با استفاده از مدلی درجه دوم بر اساس طرح مرکب مرکزی بهینه شد. آنالیزهای آماری نشان داد که هر دو متغیر نقش مهمی در فرایند جذب کادمیوم ایفا می‌کنند. بیشترین جذب کادمیوم، یعنی ۹۹/۲۴٪، تحت شرایط عملیاتی بهینه شامل pH برابر ۱۱ و نسبت نانوکامپوزیت/فلز ۹۰ پس از ۲ ساعت جذب تعادلی به دست آمد. بررسی سینتیک جذب نشان داد که جذب بیشینه طی مدت کوتاه حدود ۲ دقیقه‌ای و طبق مدل مرتبه اول حاصل می‌شود. مطالعه ایزوترم‌های جذب نیز نشان داد که جذب کادمیوم بر روی نانوکامپوزیت  $Fe_3O_4$ /باطله زغال با بهترین تطابق در مقایسه با سایر مدلها، از مدل همدمای تمکین و با مکانیزم کاهش خطی گرمای جذب پیروی می‌کند. رفتار کلی حذف نیز به یک فرایند دو مرحله‌ای شامل جذب اولیه سریع کادمیوم بر روی نقاط فعال بر روی سطح نانوکامپوزیت و سپس، رسوب آهسته هیدروکسید کادمیوم در میان حفرات موجود بر سطح نانوکامپوزیت نسبت داده شد.

**کلمات کلیدی:** باطله زغال، نانوذرات  $Fe_3O_4$ ، نانوکامپوزیت، کادمیوم، سینتیک، مدل‌سازی.